SCIENTIFIC REPORTS

OPEN

SUBJECT AREAS:
METAL-ORGANIC FRAMEWORKS
LASERS, LEDS AND LIGHT SOURCES

Received
3 December 2013

Accepted
18 February 2014

Published
11 March 2014

Correspondence and requests for materials should be addressed to D.P.Y. (yandongpeng001@163.com; yandp@mail.buct.edu.cn)

Tunable Two-color Luminescence and Host–guest Energy Transfer of Fluorescent Chromophores Encapsulated in Metal-Organic Frameworks

Dongpeng Yan[1,2], Yanqun Tang[2], Heyang Lin[2] & Dan Wang[2]

[1]Key Laboratory of Theoretical and Computational Photochemistry, Ministry of Education, College of Chemistry, Beijing Normal University, Beijing 100875, China, [2]State Key Laboratory of Chemical Resource Engineering, Beijing University of Chemical Technology, Beijing 100029, P. R. China.

Co-assembly of chromophore guests with host matrices can afford materials which have photofunctionalities different from those of individual components. Compared with clay and zeolite materials, the use of metal–organic frameworks (MOFs) as a host structure for fabricating luminescent host–guest materials is still at an early stage. Herein, we report the incorporation of a laser dye, 4-(dicyanomethylene)-2-methyl-6-(4-dimethylaminostyryl)-4H-pyran (DCM), into stilbene-based and naphthalene-based MOF systems. The resulting materials exhibit blue/red two-color emission, and the intensity ratio of blue to red fluorescence varies in different planes within the MOF crystal as detected by 3D confocal fluorescence microscopy. The observed changes in ratiometric fluorescence suggest the occurrence of energy transfer from MOF host to DCM molecules, which can be further confirmed by periodic density functional theoretical (DFT) calculations. Moreover, selective changes in luminescence behavior are observed on treating the guest@MOF samples with volatile organic compounds (methanol, acetone and toluene), indicating that these host–guest systems have potential applications as fluorescence sensors. It can be expected that by rational selection of MOF hosts and guest chromophores with suitable emissive colors and energy levels, a wide variety of multi-color luminescent and energy-transfer systems can readily be prepared in a similar manner.

The incorporation of fluorescent guest molecules into the nanochannels of host matrices has attracted much recent attention in terms of both fundamental studies and the development of applications in light emitting diodes[1], polarized emission[2], lasers[3], and other optoelectronic devices[4]. As a result of host–guest interactions and collective effects, the resulting organized assemblies can also display unique functionalities (such as emission properties and photo-/thermal-stabilization) which are not simply the sum of those of the individual components[5]. Metal–organic frameworks (MOFs), also known as coordination polymers, are a class of regular crystalline solids with intrinsically well-organized host structures formed by the coordination of metal cations/clusters with organic units[6–9]. Recently, functional MOFs have been shown to have potential applications in many areas including gas storage/separation[10,11], catalysis[12,13], non-linear optics[14], and magnetism[15,16]. In addition, organic ligand-based luminescent MOFs have also been developed as fluorescence sensors during the last decade[17–28]. To date, compared with other host frameworks (such as one-dimensional (1D) nanotubes[29], two-dimensional (2D) layered clays[30] and three-dimensional (3D) zeolite materials[31]), the study of the encapsulation of guest chromophores into 3D MOFs is still in its infancy and examples are limited[32–34]. Therefore, how to rationally design suitable host porous topologies and select the guest species remains a major goal[35]. In addition, by introduction of chromophores with different emission properties into the MOF crystals, it should be possible to construct two-color luminescent systems for ratiometric fluorescence applications[36].

4-(Dicyanomethylene)-2-methyl-6-(4-dimethylaminostyryl)-4H-pyran (DCM, Figure 1A) is a well-known laser dye, which has attracted considerable attention as a red-color emissive material due to its high photoluminescent quantum yield and excellent optical and electronic properties[37]. In this work, we chose DCM as the fluorescent guest, and stilbene-based and naphthalene-based MOFs (stilbene-MOF[38] and naphthalene-MOF (also known as IRMOF-8[39]), Figure 1B and 1C) as the host matrices. Both stilbene-MOF and naphthalene-

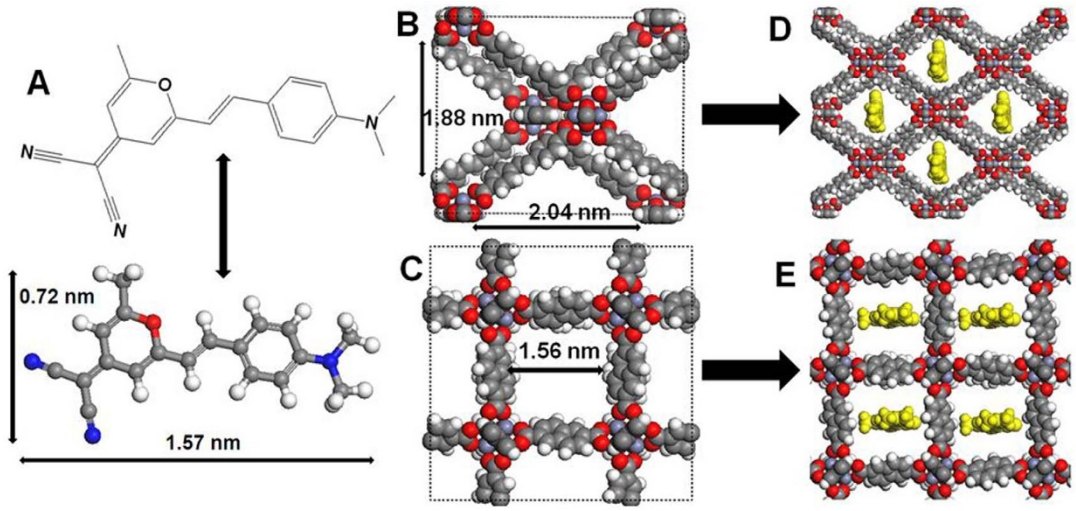

Figure 1 | Incorporation of DCM guests into the nanochannels of MOFs. (A) The molecular structure of DCM; the host structures of stilbene-MOF (B) and IRMOF-8 (C); the schematic host–guest structures of DCM@stilbene-MOF (D) and DCM@IRMOF-8 (E).

MOF are based on zinc carboxylate units of the type $Zn_4O(O_2C–R–CO_2)_3$, where the linker –*R*– is trans-4,4′-stilbene in the former and 2,6-napthalene in the latter. These were chosen as host materials because they both have large porous channels (1.88 nm × 2.04 nm and 1.56 nm × 1.56 nm, respectively) and are easy to prepare. When irradiated by UV light, stilbene-MOF and naphthalene-MOF emit in the blue–violet region. Under sonication both materials were able to encapsulate DCM and the resulting DCM@MOFs (Figure 1D and 1E) exhibited well-defined blue/red two-color emission, in which the intensity ratio of blue to red fluorescence can be varied in different regions within the MOF crystal. Moreover, the ratiometric fluorescence can also be tuned by treatment with volatile organic compounds (VOCs), indicating that these host–guest systems have potential applications as fluorescence sensors.

Results and discussion

The host structures of stilbene-MOF and IRMOF-8 were synthesized by hydrothermal methods, and the powder X-ray diffraction (XRD) patterns for their as-obtained crystals are shown in Figure 2. In each case, the reflections fit well with the patterns simulated using the single-crystal structures[38,39], confirming the high purity of the samples. Crystals of the pristine stilbene-MOF and IRMOF-8 were transparent in daylight (Figures 3a and 3e, respectively) and exhibited blue-violet emission under UV light (Figures 3b and 3f, respectively). Upon incorporation of DCM molecules within the pores of the stilbene-MOF and IRMOF-8 induced by sonication, the characteristic peaks maintain nearly the same positions as those of pristine MOFs (Figure 2), confirming the samples have the same host frameworks as the initial crystals. For the DCM@stilbene-MOF (Figure 2A), the increase in the relative intensity of the (121) diffraction peak may suggest that the linear DCM molecules are most likely arranged in the (121) direction of the MOF channel, which results in the high electronic density in this direction. To further understand the adsorption sites of the DCM within the MOFs, low-temperature (77 K) N_2 sorption measurements were performed on the MOF samples before and after the encapsulation of DCM molecules, and the typical N_2 sorption isotherms for the two samples are shown in Figure S1 in Electronic Supplementary Information (ESI). The as-obtained Brunauer-Emmett-Teller (BET) specific surface area of the stilbene-MOF is 898.8 m^2/g, which is relative higher than that of the previous estimated value (580 m^2/g)[38]; the BET surface area of the IRMOF-8 is 1021.7 m^2/g, which is comparable with previously reported IRMOF series structures[39]. These results confirm

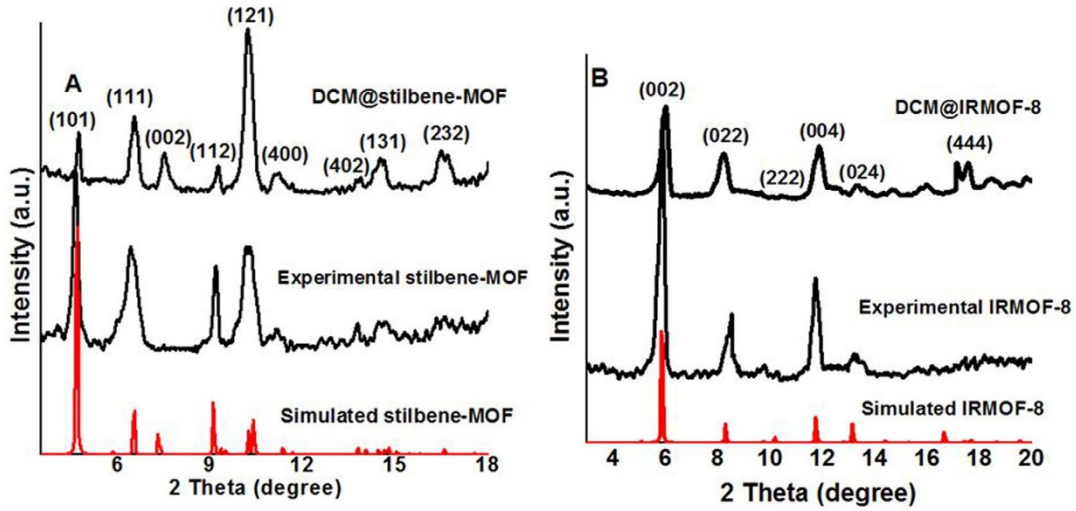

Figure 2 | Comparison of the experimental powder XRD patterns of stilbene-MOF and DCM@ stilbene-MOF (A), and IRMOF-8 and DCM@IRMOF-8 (B) with the results simulated on the basis of the single-crystal structures.

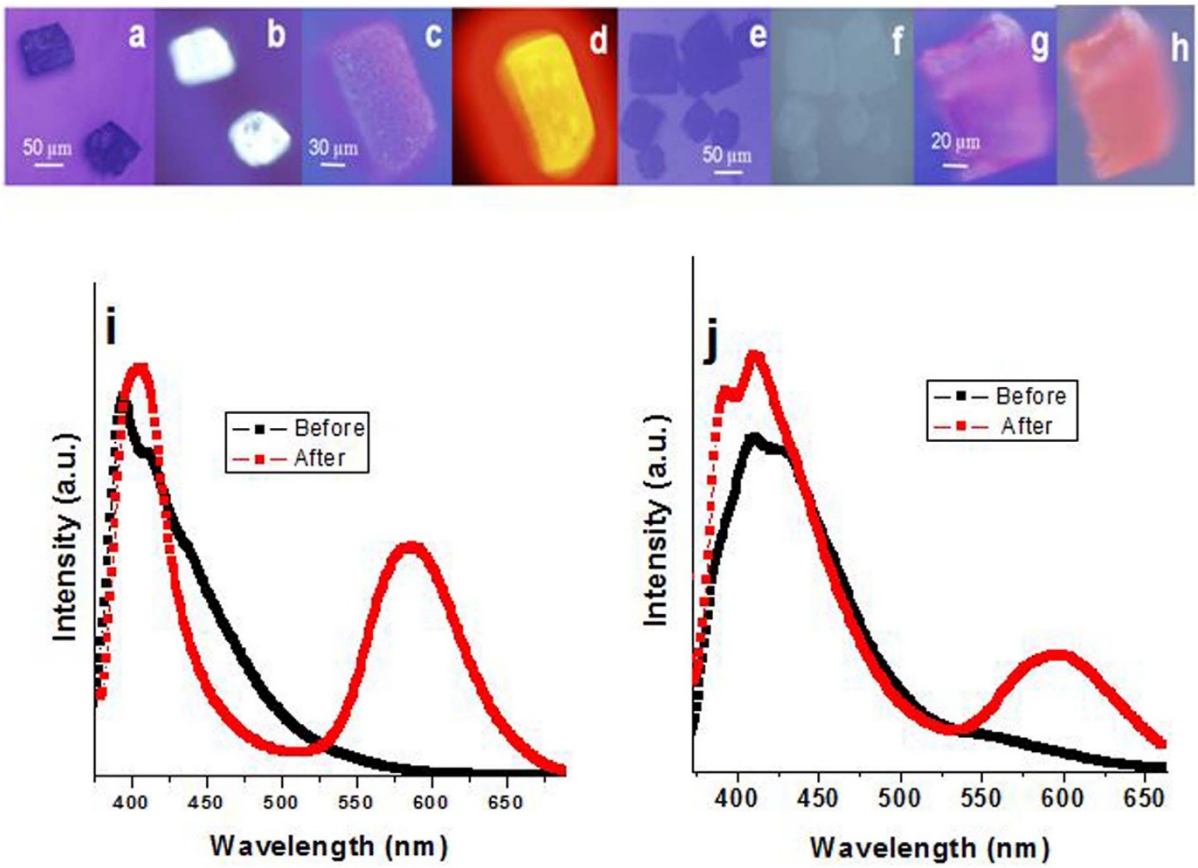

Figure 3 | Photographs of crystals of pure stilbene-MOF (a), (b) and IRMOF-8 (e), (f), DCM@stilbene-MOF (c), (d) and DCM@IRMOF-8 (g), (h) under daylight (a), (c), (e), (g) and UV irradiation (b), (d), (f), (h) observed using a fluorescence microscope; the fluorescence spectra of stilbene-MOF (i) and IRMOF-8 (j) samples before and after modification with DCM.

the porosity of these frameworks. In addition, the average pore radiuses are 1.19 and 1.05 nm for stilbene-MOF and IRMOF-8 respectively, which is consistent with their microporous structures. However, upon encapsulation of DCM molecules, the BET specific surface area values are highly reduced to 6.9 and 15.8 m^2/g, respectively, indicating that the DCM molecules are highly absorbed into the inner pores of the MOF crystals, but not the surface of the MOF samples.

The modified stilbene-MOF and IRMOF-8 exhibited a pink color in daylight (Figures 3c and 3g, respectively), and red emission under a fluorescence microscope (Figures 3d and 3h, respectively), indicative of the successful encapsulation of DCM molecules within the MOF host structures. Compared with the pure MOFs with the emission positions at *ca.* 405 and 410 nm respectively, new emission bands of the DCM@stilbene-MOF and DCM@IRMOF-8 appeared at *ca.* 590 nm (Figure 3i and 3j), which results in blue/red two-color luminescence with intensity ratios of 1.78 and 3.57 respectively. Figures 4a and 4b and Figures S2a and S2b (ESI) show typical scanning electron microscopy (SEM) images of the micro-sized stilbene-MOF and IRMOF-8 crystals, which exhibit regular and uniform surface morphology under high-magnification. No obvious changes in the size and shape of the crystals were observed on formation of DCM@stilbene-MOF (Figures 4c and 4d) and DCM@IRMOF-8 (Figure S2c and S2d in the ESI), showing that the MOF crystals maintain their host structure and morphology during the encapsulation of DCM.

The power-dependent emission spectra of the DCM@MOF samples were further measured and compared with those of the bulk. Upon excitation by a laser at 372 nm, both the DCM@stilbene-MOF and DCM@IRMOF-8 microcrystalline samples showed increasing fluorescence brightness with increasing excitation intensity as shown in Figure 5 and Figure S3 in the ESI. The main two-color emission peaks of the DCM@stilbene-MOF and DCM@IRMOF-8 appear at approximately 410/581 and 419/587 nm, respectively. Their emission intensities correlate nearly linearly with the excitation power (inset plots in Figure 5 and Figure S3 in the ESI), showing that a one-phonon emission process is involved. To better understand the detailed spatial distribution and local emission behavior of the DCM within the MOF crystals, confocal fluorescence microscopy was employed to obtain the 3D images at the single-crystal level. Figure 6a shows a typical 3D visualization of the DCM@stilbene-

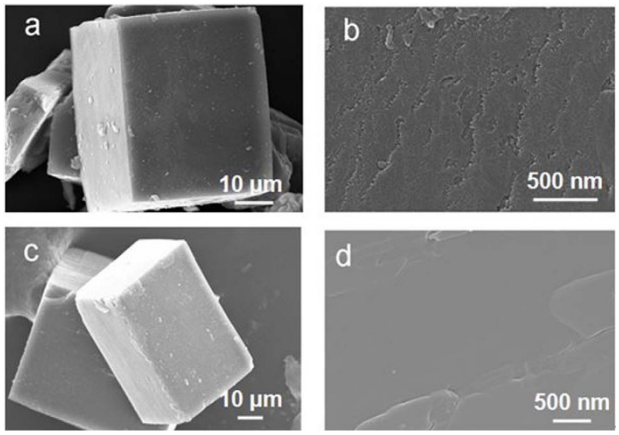

Figure 4 | Low-magnification and high-magnification SEM images for (a), (b) pristine stilbene-MOF and (c), (d) DCM@stilbene-MOF.

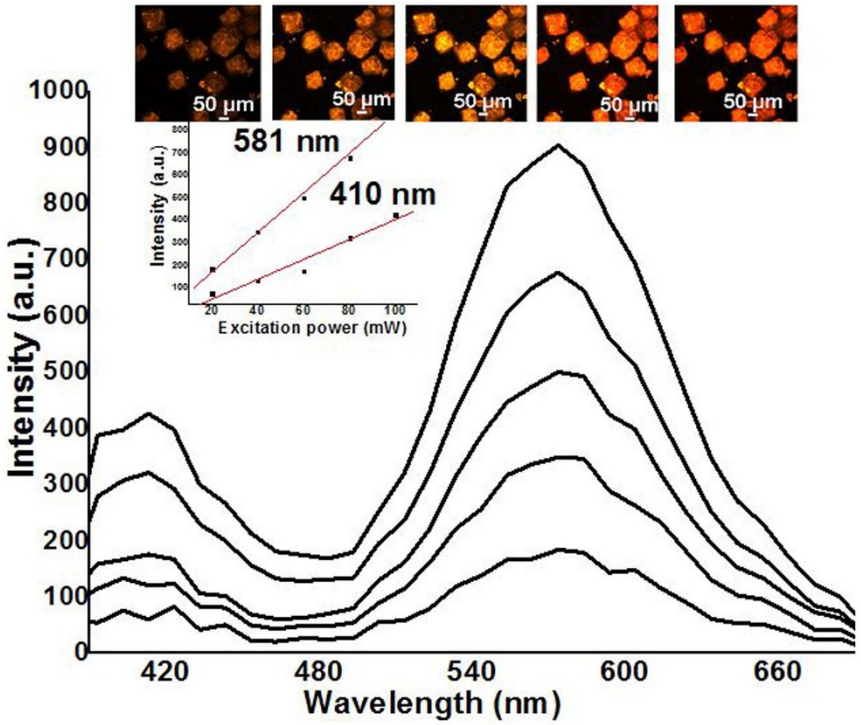

Figure 5 | Fluorescence spectra and corresponding fluorescence microscope images (inset plots) for DCM@stilbene-MOF excited by a laser (20, 40, 60, 80, 100 mW) at 372 nm. Inset shows the emission intensity at 581 and 410 nm dependent on the excitation power.

MOF, from which it can be observed that the size of the MOF crystals is uniform in the *z*-axis direction. To obtain information about emission from the crystal interior, scanning of the *xy*-plane in the *z*-axis direction was performed. The fluorescence images at five typical selected confocal *xy*-planes (inset of Figure 6b) show that the DCM molecules are almost located in the interior of the MOF crystal. Typical fluorescence spectra for different planes of an individual DCM@stilbene-MOF crystal are shown in Figure 6b. Upon increasing the distance between the focal plane and the excitation source, the intensity of the two-color emission exhibits different trends in the blue and red regions: the emission at *ca.* 410 nm first increases to a maximum as the focal plane is moved close to the centre of the MOFs, then gradually decreases as the focal plane is moved away from the centre, whilst the emission at *ca.* 581 nm decreases monotonically. This behavior can be attributed to the non-uniform distribution of the DCM within the MOFs matrix, which gives rise to differences in the energy transfer between the MOF host and DCM guest molecules: more DCM molecules are populated into the nanochannel away from the central plane of the MOF crystal than in the central plane itself, and as a result, the energy transfer from host matrix to DCM species is more effective[40]. The energy transfer efficiency can be estimated based on the intensity ratio I_{410}/I_{581}, which increases from 0.25 (z = 33 μm) to 0.81 (z = 92 μm), and then decreases to 0.19 (z = 151 μm) as illustrated in the inset of Figure 6b. A similar variation in the two-color luminescence within the crystal can also be observed for the DCM@IRMOF-8 system (Figure S4 and S5 in ESI), suggesting that such non-uniform energy transfer may be a general phenomenon for chromophore-assembled MOF host–guest structures.

To further understand the geometric/electronic structures and host–guest interactions in the crystal interior, periodic density functional theoretical (DFT) calculations were carried on the idealized model structures of DCM@stilbene-MOF and DCM@IRMOF-8. The calculation results indicate that there is no obvious change in the optimized configuration of the MOF host structures after incorporation of DCM guest molecules. Moreover, the total electronic

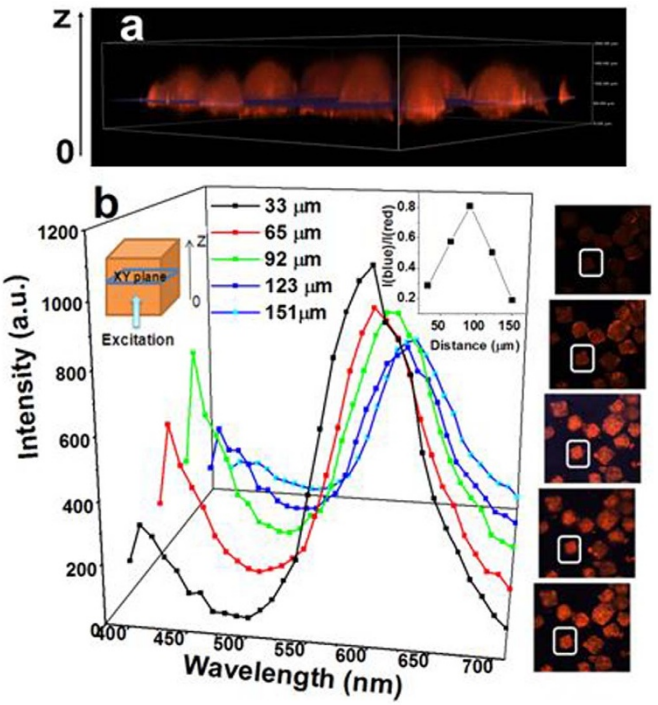

Figure 6 | (a) 3D fluorescence image of the selected single crystal MOFs; (b) the two-color fluorescence spectra and intensity ratios of blue to red emission (inset) of an individual DCM@stilbene-MOF single crystal (outlined by the white color in the inset of b) in different *xy*-planes based on *z*-axis scanning. Inset photographs show the fluorescence images in focal planes at different distances (33, 65, 92, 123, and 151 μm) from the excitation laser (372 nm).

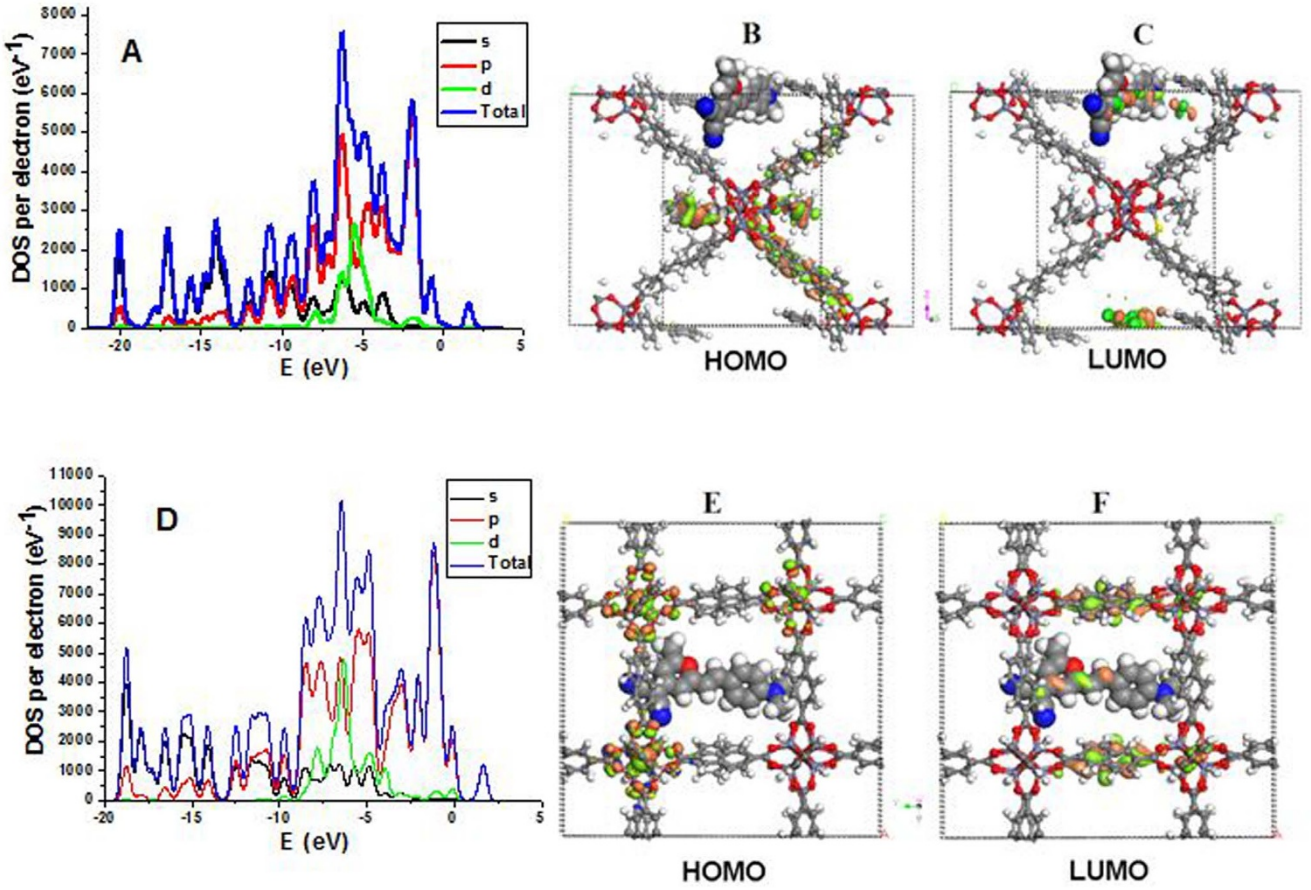

Figure 7 | Total and partial electronic density of state (TDOS and PDOS) and HOMO/LUMO for the optimized DCM@stilbene-MOF (A), (B), (C) and DCM@IRMOF-8 (D), (E), (F) structures. The Fermi energy level E_F was set to zero; the two colors green/orange denote +/− wave functions.

densities of states (TDOS) and partial electronic densities of states (PDOS) analyses (Figure 7A and Figure S6 in ESI) reveal that, for the DCM@stilbene-MOF system, the electron density of the highest occupied molecular orbitals (HOMOs) is mainly distributed on the C atoms in the stilbene units, while that of the lowest unoccupied molecular orbitals (LUMOs) is mainly located on the C and N atoms in the DCM guest molecule. Around the Fermi level, the TDOS mainly consists of the 2p electrons of conjugated C atoms in stilbene-MOF. For the DCM@IRMOF-8 structure (Figure 7D and Figure S7), the HOMOs are mainly localized on the Zn_4O cluster, and LUMOs mainly on the C/N atoms in DCM and the C atoms in naphthalene units. The frontier orbital distribution is illustrated in Figures 7B, 7C, 7E, and 7F. The calculation results clearly confirm the occurrence of energy transfer from host to guest molecules in the excitation process. Moreover, the electronic structures and energy transfer processes in the luminescent assemblies can be engineered and modified by choosing appropriate photoactive MOF host materials, which can further influence the optical properties.

In order to study potential applications of the two-color ratiometric emission of the two DCM@MOF systems in sensors, the luminescence was studied after treating with typical VOCs (methanol, acetone and toluene). Taking the DCM@stilbene-MOF as an example (Figure 8a), after exposure to VOCs the luminescence peak at 405 nm exhibited a red-shift accompanied by an increase in the emission intensity at ca. 587 nm, with the effect being the most significant for toluene. The values of intensity ratio between the blue and red luminescence were 1.14, 0.74, and 0.60 for methanol, acetone and toluene respectively. Unlike other MOF systems with solvatochromic property[33], such a selective solvent-responsive change in ratiometric luminescence can be attributed to the influence of the inclusion of different solvent molecules within the MOF channels on the host–guest energy transfer efficiency between the host matrix and the guest molecules. The blue/red emission intensity ratios for the DCM@IRMOF-8 system also varied on exposure to different VOCs (Figure 8b), suggesting that both of the DCM@MOFs can serve as new type of ratiometric luminescent sensors for VOCs.

Conclusion

DCM guest chromophores have been encapsulated within the nanopores of stilbene-MOF and IRMOF-8 host matrices, and the resulting host–guest materials exhibit blue/red two-color emission. Confocal fluorescence microscopy affords 3D visualization at the single-crystal level for the two DCM@MOF systems, and an *xy*-plane scan shows the difference in the intensity ratios of the blue : red luminescence in different focal planes of the MOF crystals, arising from the different degrees of energy transfer between the MOF hosts and guest molecules. DFT calculations confirm that host–guest energy transfer occurs for two DCM@MOF systems. Moreover, the luminescence response of the DCM@MOF systems is sensitive to volatile organic solvents, in that both the emission wavelength and the intensity ratio of blue to red emission vary after exposure, showing that the materials have potential applications in the fabrication of ratiometric luminescent sensors. The combination of experimental and theoretical studies of the DCM@MOF systems described here offers a detailed understanding of the two-color luminescence and host–guest energy transfer between the MOF matrix and the DCM chromophore. It can be anticipated that, by appropriate choice of MOF host and guest chromophores with suitable emissive colors and energy levels, a wide variety of other multi-color luminescent assemblies can readily be obtained.

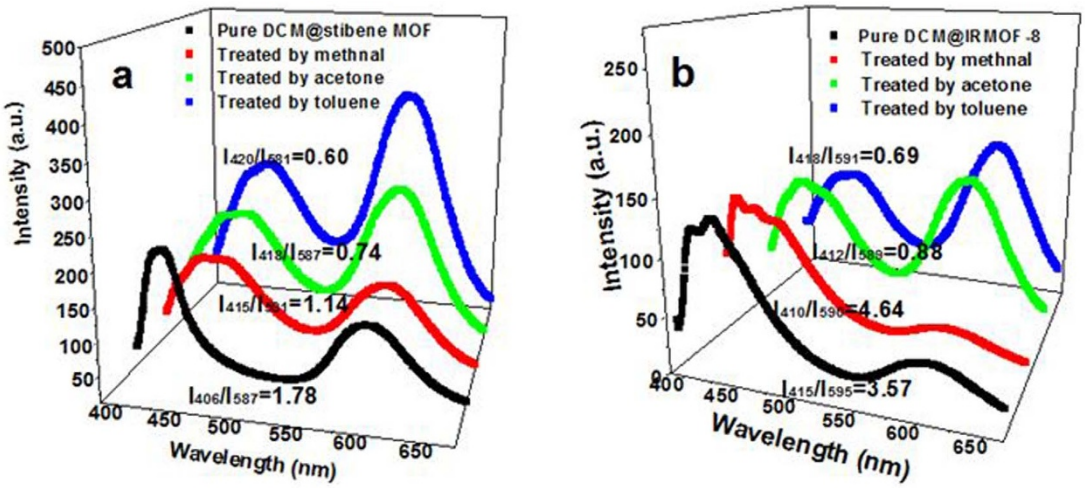

Figure 8 | Fluorescence spectra of the (a) DCM@stilbene-MOF and (b) DCM@IRMOF-8 treated with methanol, acetone and toluene.

Methods

Reagents and materials. Analytically pure $Zn(NO_3)_2 \cdot 6H_2O$, 1,4-stilbenedicarboxylic acid (H_2SDC), 2,6-naphthalenedicarboxylic acid (H_2DNC) and 4-(dicyanomethylene)-2-methyl-6-(4-dimethylaminostyryl)-4H-pyran (DCM) were purchased from Sigma Chemical Co. Ltd. and used without further purification.

Preparation of stilbene-MOF, IRMOF-8, DCM@stilbene-MOF and DCM@IRMOF-8. The stilbene-MOF and IRMOF-8 microcrystalline materials were prepared following the methods of Bauer *et al.*[38] and Eddaoudi *et al.*[39], with some small modifications. For stilbene-MOF, 0.418 g of $Zn(NO_3)_2 \cdot 6H_2O$ and 0.061 g of H_2SDC were dissolved in 50 mL of *N*,*N*-dimethylformamide (DMF), and the solution sealed in a 90 mL Teflon-lined stainless steel autoclave, and heated at 100°C for 20 hours. For IRMOF-8, 0.297 g of $Zn(NO_3)_2 \cdot 6H_2O$ and 0.108 g of H_2DNC were dissolved in 60 mL of DMF, and the solution sealed in a 90 mL Teflon-lined stainless steel autoclave, and heated at 100°C for 16 hours. The resulting products, stilbene-MOF and IRMOF-8, were washed with DMF. To prepare DCM@stilbene-MOF and DCM@IRMOF-8, 0.067 g of stilbene-MOF or 0.067 g of IRMOF-8 microcrystals was added to 50 mL of DMF containing 0.096 g of DCM and the solutions ultrasonicated for 1 hour. The products were washed thoroughly with DMF until no fluorescence was observed in the washings, and then dried at 180°C for 2 days to remove the co-assembled DMF in the pore of MOFs. All the samples were stored under vacuum. Elemental analysis gave C 48.8%, H 2.2%, N 0.8% and C 55.4%, H 3.1%, N 1.2% for the DCM@stilbene-MOF and DCM@IRMOF-8 samples respectively. Therefore, the calculated amounts of fluorescent guest molecules are 5.5% and 8.0%, respectively and the corresponding molecular formulae can be expressed as $Zn_4O(C_{12}H_6O_4)_3(C_{19}H_{16}N_3O)_{0.18}$ and $Zn_4O(C_{16}H_{10}O_4)_3(C_{19}H_{16}N_3O)_{0.31}$, respectively.

Sample characterization. X-ray diffraction patterns (XRD) of samples were recorded using a Rigaku 2500VB2 + PC diffractometer under the following conditions: 40 kV, 50 mA, Cu Kα radiation ($\lambda = 0.154056$ nm) with step-scanning in steps of 0.04° (2θ) in the range 3 to 20° using a count time of 10 s/step. C, H, N analyses were carried out using a Elementar Vario elemental analyzer. The morphology was investigated by using a scanning electron microscope (SEM, Hitachi S-3500) equipped with an energy-dispersive X-ray (EDX) attachment (Oxford Instruments Isis 300), with an acceleration voltage of 20 kV. Low-temperature (77 K) N_2 adsorption–desorption measurements were performed on a Micromeritics ASAP 2020 instrument. The specific surface areas were calculated based on the Brunauer-Emmett-Teller (BET) method, and pore size distributions were obtained by a nonlocal Density Functional Theory model. The solid-state fluorescence spectra were recorded on RF-5301PC fluorospectrophotometer, with the widths of both the excitation and emission slits being 3 nm. The fluorescence images were obtained with a Nikon A1R-si laser scanning confocal microscope, and a galvano scanner was used to capture high-quality 32-channel spectral images.

Calculation details. *Building of the structural models for guest@MOF systems and calculation methods.* The ideal stilbene-MOF and IRMOF-8 crystal structures with R3*m* space group are derived from the results of Bauer *et al.*[38] and Eddaoudi *et al.*[39], in which $a = 30.317$ Å, $b = 19.411$ Å, $c = 24.161$ Å and $\alpha = \beta = \gamma = 90°$ for stilbene-MOF and $a = b = c = 30.0915$ Å, and $\alpha = \beta = \gamma = 90°$ for IRMOF-8. The supercells were further treated as P1 symmetry, and a 3D periodic boundary condition was applied. Then, DCM molecules can be introduced into the pores of the stilbene-MOF and IRMOF-8. The formula of the calculated structures for the guest@MOF systems can be expressed as: $Zn_{32}O_8(C_{12}H_6O_4)_{24}(C_{19}H_{16}N_3O)$ and $Zn_{16}O_4(C_{16}H_{10}O_4)_{12}(C_{19}H_{16}N_3O)$. All calculations were performed with the periodic density functional theory (DFT) method using the DMol^3 module[41] in the Materials Studio software package[42]. The initial configuration was fully optimized by the Perdew–Wang (PW91)[43] generalized gradient approximation (GGA) method with double numerical basis sets plus polarization function (DNP). The core electrons for metals were treated by effective core potentials (ECP). The SCF convergence criterion was within 1.0×10^{-5} hartree/atom and the convergence criterion of the structure optimization was 1.0×10^{-3} hartree/bohr. The Brillouin zone was sampled by $1 \times 1 \times 1$ *k*-points, and test calculations revealed that an increase in *k*-points did not affect the results.

1. Lee, T.-W., Park, O. O., Yoon, J. & Kim, J.-J. Polymer-layered silicate nanocomposite light-emitting devices. *Adv. Mater.* **13**, 211–213 (2001).
2. Busby, M., Kerschbaumer, H., Calzaferri, G. & De Cola, L. Orthogonally bifunctional fluorescent zeolite-L microcrystals. *Adv. Mater.* **20**, 1614–1618 (2008).
3. Benedict, J. B. *et al.* Up-conversion luminescence in dye-doped crystals of potassium hydrogen phthalate. *Adv. Mater.* **15**, 1068–1070 (2003).
4. Agranovich, V. M., Gartstein, Y. N. & Litinskay, M. Hybrid resonant organic–inorganic nanostructures for optoelectronic applications. *Chem. Rev.* **111**, 5179–5214 (2011).
5. McCulloch, I. *et al.* Liquid-crystalline semiconducting polymers with high charge-carrier mobility. *Nat. Mater.* **5**, 328–333 (2006).
6. Eddaoudi, M. *et al.* Modular chemistry: secondary building units as a basis for the design of highly porous and robust metal–organic carboxylate frameworks. *Acc. Chem. Res.* **34**, 319–330 (2001).
7. Lin, W. Homochiral porous metal–organic frameworks: why and how? *J. Solid State Chem.* **178**, 2486–2490 (2005).
8. Férey, G. Hybrid porous solids: past, present, future. *Chem. Soc. Rev.* **37**, 191–241 (2008).
9. Murray, L. J., Dincá, M. & Long, J. R. Hydrogen storage in metal–organic frameworks. *Chem. Soc. Rev.* **38**, 1294–1314 (2009).
10. Ma, S., Sun, D., Wang, X. S. & Zhou, H.-C. A mesh-adjustable molecular sieve for general use in gas separation. *Angew. Chem. Int. Ed.* **46**, 2458–2462 (2007).
11. Lu, G. *et al.* Imparting functionality to a metal–organic framework material by controlled nanoparticle encapsulation. *Nat. Chem.* **4**, 310–316 (2012).
12. Seo, J. S. *et al.* A homochiral metal–organic porous material for enantioselective separation and catalysis. *Nature* **404**, 982–986 (2000).
13. Huang, Y. & Lin, Z. Palladium nanoparticles encapsulated in a metal–organic framework as efficient heterogeneous catalysts for direct C2 arylation of indoles. *Chem. Eur. J.* **17**, 12706–12712 (2011).
14. Zhou, W.-W. *et al.* Nonlinear optical and ferroelectric properties of a 3-D Cd(II) triazolate complex with a novel $(6^3)_2(6^{10} \cdot 8^5)$ topology. *Chem. Commun.* 2762–2764 (2008).
15. Wang, W. *et al.* Magnetoelectric coupling in the paramagnetic state of a metal–organic framework. *Sci. Rep.* **3**, 2024; DOI:10.1038/srep02024 (2013).
16. Ohba, M., Yoneda, K. & Kitagawa, S. Guest-responsive porous magnetic frameworks using polycyanometallates. *CrysEngComm.* **12**, 159–165 (2010).
17. Cui, Y., Yue, Y., Qian, G. & Chen, B. Luminescent functional metal–organic frameworks. *Chem. Rev.* **112**, 1126–1162 (2012).
18. Kreno, L. E. *et al.* Metal–organic framework materials as chemical sensors. *Chem. Rev.* **112**, 1105–1125 (2012).
19. Allendorf, M. D., Bauer, C. A., Bhakta, R. K. & Houk, R. J. T. Luminescent metal–organic frameworks. *Chem. Soc. Rev.* **38**, 1330–1352 (2009).
20. Stylianou, K. C. *et al.* A guest-responsive fluorescent 3D microporous metal-organic framework derived from a long-lifetime pyrene core. *J. Am. Chem. Soc.* **132**, 4119–4130 (2010).

21. Grünker, R. *et al.* Topological Diversity, Adsorption and fluorescence properties of MOFs based on a tetracarboxylate ligand. *Eur. J. Inorg. Chem.* **24**, 3835–3841 (2010).
22. Ma, J. P., Yu, Y. & Dong, Y. B. Fluorene-based Cu (ii)-MOF: a visual colorimetric anion sensor and separator based on an anion-exchange approach. *Chem. Commun.* **48**, 2946–2948 (2012).
23. Chen, B., Xiang, S. & Qian, G. Metal−organic frameworks with functional pores for recognition of small molecules. *Acc. Chem. Res.* **43**, 1115–1124 (2010).
24. Rocha, J. *et al.* Luminescent multifunctional lanthanides-based metal–organic frameworks. *Chem. Soc. Rev.* **40**, 926–940 (2011).
25. Lee, H., Jung, S. H. & Han, W. S. A chromo-fluorogenic tetrazole-based $CoBr_2$ coordination polymer gel as a highly sensitive and selective chemosensor for volatile gases containing chloride. *Chem. Eur. J.* **17**, 2823–2827 (2011).
26. Zhu, Q. L. *et al.* Redox-responsive photochromism and fluorescence modulation of two 3D metal organic hybrids derived from a triamine-based polycarboxylate ligand. *Chem. Eur. J.* **17**, 3358–3362 (2011).
27. Takashima, Y. *et al.* Molecular decoding using luminescence from an entangled porous framework. *Nat commun.* **2**, 168–176 (2011).
28. Stylianou, K. C. *et al.* A guest-responsive fluorescent 3D microporous metal-organic framework derived from a long-lifetime pyrene core. *J. Am. Chem. Soc.* **132**, 4119–4130 (2010).
29. Yanagi, K. *et al.* Photosensitive function of encapsulated dye in carbon nanotubes. *J. Am. Chem. Soc.* **129**, 4992–4997 (2007).
30. Yan, D. P. *et al.* Layered host–guest materials with reversible piezochromic luminescence. *Angew. Chem. Int. Ed.* **50**, 7037–7040 (2011).
31. Cucinotta, F. *et al.* Microcontact transfer printing of zeolite monolayers. *Adv. Mater.* **21**, 1142–1145 (2009).
32. Yanai, N. *et al.* Gas detection by structural variations of fluorescent guest molecules in a flexible porous coordination polymer. *Nat. Mater.* **10**, 787–793 (2011).
33. Grünker, R. *et al.* Dye Encapsulation inside a new mesoporous metal–organic framework for multifunctional solvatochromic-response function. *Chem. Eur. J.* **18**, 13299–13303 (2012).
34. Yanai, N., Uemura, T. & Inoue, M. Guest-to-host transmission of structural changes for stimuli-responsive adsorption property. *J. Am. Chem. Soc.* **134**, 4501–4504 (2012).
35. Yan, D., Lloyd, G. O., Delori, A., Jones, W. & Duan, X. Tuning fluorescent molecules by inclusion in a metal–organic framework: an experimental and computational study. *ChemPlusChem* **77**, 1112–1118 (2012).
36. Sun, C. *et al.* Efficient and tunable white-light emission of metal–organic frameworks by iridium-complex encapsulation. *Nat. Commun.* **4**, 2717–2724 (2013).
37. Kan, S. *et al.* Improved efficiency of single-layer polymer light-emitting devices with poly(vinylcarbazole) doubly doped with phosphorescent and fluorescent dyes as the emitting layer. *Adv. Funct. Mater.* **13**, 603–608 (2003).
38. Bauer, C. A. *et al.* Influence of connectivity and porosity on ligand-based luminescence in zinc metal-organic frameworks. *J. Am. Chem. Soc.* **129**, 7136–7144 (2007).
39. Eddaoudi, M. *et al.* Systematic design of pore size and functionality in isoreticular MOFs and their application in methane storage. *Science* **295**, 469–472 (2002).
40. Nguyen, T.-Q., Wu, J. J., Doan, V., Schwartz, B. J. & Tolbert, S. H. Control of energy transfer in oriented conjugated polymer–mesoporous silica composites. *Science* **288**, 652–656 (2000).
41. Delley, B. From molecules to solids with the $DMol^3$ approach. *J. Chem. Phys.* **113**, 7756–7764 (2000).
42. $DMol^3$ Module, *MS Modeling*, Version 2.2; Accelrys Inc.: San, Diego, CA, 2003.
43. Perdew, J. P. *et al.* Atoms, molecules, solids, and surfaces: applications of the generalized gradient approximation for exchange and correlation. *Phys. Rev. B* **46**, 6671–6683 (1992).

Acknowledgments

This work was supported by the 973 Program (Grant no. 2014CB932103), the National Natural Science Foundation of China (NSFC), the Scientific Fund from Beijing Municipal Commission of Education (20111001002), the Fundamental Research Funds for the Central Universities and the 111 Project (Grant B07004).

Author contributions

D.Y. has designed the experiments, performed the synthesis and computational simulations, interpreted the data and co-wrote the paper. Y.T. carried out the structure and adsorption characterizations and data analysis. H.L. and D.W. performed the fluorescence images. All authors discussed and commented on the manuscript.

Additional information

Supplementary information accompanies this paper at http://www.nature.com/scientificreports

Competing financial interests: The authors declare no competing financial interests.

How to cite this article: Yan, D.P., Tang, Y.Q., Lin, H.Y. & Wang, D. Tunable Two-color Luminescence and Host–guest Energy Transfer of Fluorescent Chromophores Encapsulated in Metal-Organic Frameworks. *Sci. Rep.* **4**, 4337; DOI:10.1038/srep04337 (2014).